mathematics

MDPI

Article

An Enhanced Hybrid-Level Interface-Reduction Method Combined with an Interface Discrimination Algorithm

Seunghee Cheon and Jaehun Lee *

Department of Mechanical Engineering, Dongguk University, Seoul 04620, Republic of Korea; s.hee.cheon@dgu.ac.kr
* Correspondence: jaehun@dgu.edu

Abstract: This study proposes an interface localizing scheme to enhance the performance of the previous hybrid-level interface-reduction method. The conventional component mode synthesis (CMS) only focuses on interior reduction, while the interface is fully retained for convenient synthesis. Thus, various interface-reduction methods have been suggested to obtain a satisfactory size for the reduced systems. Although previous hybrid-level interface-reduction approaches have addressed major issues associated with conventional interface-reduction methods—in terms of accuracy and efficiency through considering partial substructure synthesis—this method can be applied to limited modeling conditions where interfaces and substructures are independently defined. To overcome this limitation, an interface localizing algorithm is developed to ensure an enhanced performance in the conventional hybrid-level interface-reduction method. The interfaces are discriminated through considering the Boolean operation of substructures, and the interface reduction basis is computed at the localized interface level, which is constructed by a partially coupled system. As a result, a large amount of computational resources are saved, achieving the possibility of efficient design modifications at the semi-substructural level.

Keywords: parametric component mode synthesis; Craig Bampton method; interface reduction; characteristic constraint modes; hybrid-level interfaces

MSC: 70-08

check for updates

Citation: Cheon, S.; Lee, J. An Enhanced Hybrid-Level Interface-Reduction Method Combined with an Interface Discrimination Algorithm. *Mathematics* **2023**, *11*, 4867. https://doi.org/10.3390/math11234867

Academic Editor: Matjaz Skrinar

Received: 8 November 2023
Revised: 29 November 2023
Accepted: 1 December 2023
Published: 4 December 2023

Copyright: © 2023 by the authors. Licensee MDPI, Basel, Switzerland. This article is an open access article distributed under the terms and conditions of the Creative Commons Attribution (CC BY) license (https://creativecommons.org/licenses/by/4.0/).

1. Introduction

Numerical simulations for large-scale, dynamical systems are challenging tasks even now. To mitigate these computational burdens, introducing a reduced-order model (ROM) within a surrogate modeling framework can be an attractive solution. In general, reduced-order modeling is realized by projecting a full-order system into a lower subspace using a truncated reduction basis. Traditionally, the eigenvectors of a system matrix can be a projection basis that transforms the state vector into a generalized coordinate system. By truncating the eigenvectors, one achieves a dimensionality reduction in the given system. Another type of reduction is achieved through introducing the singular value decomposition of data usually obtained from a response of the system. Such dimensionality reduction is one of the general approaches in the viewpoint of a data analysis regardless of the underlying physics of the given problems. For either the data or the system, the reduction results in efficient computations, particularly for such engineering disciplines that inevitably require heavy numerical simulations.

From the viewpoint of deriving and using appropriate reduced-order models for real industrial applications, an efficient adaptation to parametric variations is one of the most important properties that the ROM should have. Thus, the model reduction techniques have been widely investigated for real industrial systems, particularly large-scale models that undergo parametric variations. The offline–online strategy [1,2] alleviated a large

amount of computation caused by repetitive evaluations with respect to parameter changes. Once a substantial amount of data is acquired in the offline stage, prediction accuracy can be increased in the online stage. One of the major barriers that hinders applying the offline–online strategy is the number of parameters that the system contains. In particular, the offline cost dramatically increases due to the sampling of the independent parameters, which is referred to as the "curse of dimensionality". To mitigate such complexities caused by the dependencies between the parameters, various sampling strategies [3,4] have been developed within the framework of surrogate modeling and the design of experiments. To be more specific, domain-decomposition-based methods have also been developed for the spatially distributed parameters [5–7]. Such approaches have shown the possibility of offline time reduction for high dimensional parameter spaces. Some works have also developed mathematical techniques to address dimensional problems for complex finite element modeling (FEM) [8–11].

The main advantage of component mode synthesis (CMS), which stands for dynamic substructuring, is that the entire system is divided into multiple independent subsystems, and model reduction is performed at a substructural level. Therefore, design modification can be practically reflected without requiring full-system analysis with respect to design-variable changes. Based on these concepts of domain decomposition, Hurty [12] was initially conceptualized by applying normal, rigid-body, and constraint modes within the finite element modeling (FEM) framework. Subsequently, Craig Bampton [13] discovered that the treatment of interface can be simplified by considering rigid-body and redundant modes in the same manner. Bennighof and Lehoucq [14] formulated an automatic multi-level substructuring method to achieve high dimensional reduction with a similar accuracy level as modal truncation. In addition, proper consideration of residual substructural modes based on a Craig Bampton (CB) method has been suggested for enhanced accuracy by Kim [15]. The efficiency and accuracy of CMS methods are demonstrated in [12–18].

The majority of engineering systems consist of multiple materials and components. For this reason, the treatment of interface is another essential consideration for efficient and robust FEM simulation due to interaction between each domain. Peskin [19] presented the immersed boundary (IB) method to handle fluid–flexible structure interactions, such as blood flow in the heart. Based on the IB method, related works handling interfaces could be found in [20–22]. According to Craig Bampton's work, a divided substructure is separately treated for reduction as interior and interface degrees of freedom (DOFs). The fixed interface normal modes (FINMs) and static constraint modes (SCMs) are independently applied to a partitioned subsystem. This approach offers the benefit of convenience synthesis, as it ensures the interface compatibility. On the other hand, the CB method has a significant disadvantage in that it requires an additional reduction method to obtain sufficiently reduced systems. The reduced subsystems are tend to be dominated by interface DOFs under several circumstances, where fine mesh or numerous subcomponents are adopted for modeling. Therefore, to achieve a manageable size of reduced system matrices, various interface reduction techniques are presented by performing two-level reduction.

Craig and Chang [23] initially proposed the concept of interface reduction by incorporating several model reductions, such as Guyan, Ritz, and modal reduction. Castanier et al. [24] developed Craig and Chang's modal reduction method as a system-level characteristic constraint (CC) mode. The interface reduction basis is computed using secondary eigenvalue analysis to a fully synthesized system. This system-level interface-reduction method successfully represents the physical motion of the interface. Due to the constant effort for highly reduced systems, the interface reduction approach is continuously extended to various engineering fields. Traditionally, Tran [25,26] applied CMS using interface modes to the cyclic symmetry problems. Herrmann et al. [27] applied Craig and Chang's work to the acoustic fluid–structure interaction and predicted hydraulic transfer system using ROM reduced by appropriate Ritz vectors. According to recent studies, Cammarata et al. [28] presented a novel interface-reduction method for interpolation multipoint constraints by discarding dependent node selection. Hughes and Kuether [29] handled

nonlinear interface for further system reduction by computing system-level CC modes and proper orthogonal interface modal derivatives. They validated this newly proposed interface reduction scheme to frictional contact system considering time transient. Additional investigations exploiting interface reduction based on dynamic substructuring to engineering fields are shown in [30–32].

The system-level CC modes approach hinders the primary advantage of CMS, which rapidly responds to parametric variations. In other words, the independence of each subsystem is no longer assured since the final reduced system is obtained after all substructures are coupled. To emphasize the flexibility of design, the local-level interface-reduction method is presented by Hong et al. [33]. The secondary eigenvalue analysis is computed at the subsystem level; exact interface compatibility should be enforced for synthesis after interface reduction. Kuether et al. [34] suggested weak compatibility at local-level interface reduction to minimize compatibility errors, constructing geometric nonlinear reduced-order models. Nevertheless, this local-level technique causes a considerable compromise in accuracy. Holzwarth et al. [35] aimed to improve the accuracy of local-level CC modes computation by adopting the Legendre polynomials. However, accuracy compromising and synthesis cumbersome remain critical concerns.

To overcome the shortcomings of the aforementioned CC modes approaches, CC modes computation to a partially synthesized system has been constantly investigated. The multilevel interface reduction presented by Wu et al. [36] performs secondary eigenvalue analysis at a localized subset level by assembling paired substructures. This method reduces computational effort and guarantees accuracy as much as the system level. Furthermore, based on the concept of Aoyama's work [37] considering a partially assembled system and separately computing CC modes, Krattiger et al. [38] recently proposed the hybrid-level (HB-level) interface reduction that allows applying boundary condition free system. These introduced methods can compromise accuracy and efficiency since constructing a single interface does not need information on disconnected substructures, but substructure connectivity is not entirely ignored. Additionally, these methods allow interface parallel computation.

Despite the CC modes computation method has substantial strengths when considering a partially synthesized system, the previous HB-level interface reduction is only applicable for modeling where each interface is independently defined and isolated. Therefore, this conventional method has difficulties in application to real industrial engineering problems. In this study, the modified HB-level interface-reduction method is proposed to provide more practical solutions for parametric studies. The proposed method aims to apply to unlimited modeling scenarios while the advantages of each localized interface set are retained. The unique numbering-based interface discrimination algorithm is integrated with the previous HB-level interface reduction [38] to address the limitation. To assess the performance of the proposed method, the graphic partitioning algorithm METIS [39] is adopted for substructuring systems. Multiple substructuring scenarios are provided to demonstrate wide applicable modeling ranges.

This paper is organized as follows. In Section 2, the CB method is described. In Section 3, the interface discrimination algorithm to build independent interface sets and a new interface reduction are proposed, with a brief review of the hybrid-level interface reduction. In Section 4, several numerical examples decomposed into multiple subdomains by METIS are presented to evaluate the performance of the proposed method.

2. Craig Bampton Method-Based Component Mode Synthesis

The conventional Craig Bampton method has been developed within the finite element discretization framework. Hence, the FEM formulation for system equation is obtained following the principle of virtual work. Further details of basic FEM formulation procedure are found in Ref. [40]. The full system equation in terms of finite element modeling is expressed as

$$\mathbf{M}\ddot{\mathbf{u}} + \mathbf{C}\dot{\mathbf{u}} + \mathbf{K}\mathbf{u} = \mathbf{f}. \tag{1}$$

Equation (1) describes the global system before performing substructuring. **M**, **C**, and **K** represent mass, damping, and stiffness matrices, respectively. **u** and **f** are the displacement and force vectors, respectively. The size of the presented entire system is N_s. Based on the classical CB method, this proposed method is applicable to the condition that the boundary DOFs is exactly separated as nodal displacement.

In the CB-CMS, the partitioning of interiors and interfaces is essential to realize straightforward synthesis. Following the global system matrices Equation (1), each subsystem matrix is written as

$$\begin{bmatrix} \mathbf{M}^s_{ii} & \mathbf{M}^s_{ib} \\ \mathbf{M}^s_{bb} & \mathbf{M}^s_{bi} \end{bmatrix} \begin{bmatrix} \ddot{\mathbf{u}}^s_i \\ \ddot{\mathbf{u}}^s_b \end{bmatrix} + \begin{bmatrix} \mathbf{K}^s_{ii} & \mathbf{K}^s_{ib} \\ \mathbf{K}^s_{bb} & \mathbf{K}^s_{bi} \end{bmatrix} \begin{bmatrix} \mathbf{u}^s_i \\ \mathbf{u}^s_b \end{bmatrix} = \begin{bmatrix} \mathbf{f}^s_i \\ \mathbf{f}^s_b \end{bmatrix}, \tag{2}$$

where

$$\mathbf{M}^s\ddot{\mathbf{u}} + \mathbf{K}^s\mathbf{u} = \mathbf{F}^s, \quad s = 1, 2, ..., N_d. \tag{3}$$

In this substructural system, the damping is ignored for convenience. The superscript s denotes the number of substructures, and the entire system is decomposed into total N_d subcomponents. The subscripts i and b indicate the degrees of freedom for interiors and boundaries known as interfaces.

For the sth subsystem reduction, the eigenvalue analysis is performed on interior DOFs to obtain fixed interface normal modes, one obtains the following FINMs:

$$\mathbf{\Phi}^s_{im} = [\boldsymbol{\phi}^s_{i,1}, \boldsymbol{\phi}^s_{i,2}, ..., \boldsymbol{\phi}^s_{i,N^s_m}], \tag{4}$$

where

$$\mathbf{K}^s_{ii}\boldsymbol{\phi}_{i,\xi} = \lambda_{i,\xi}\mathbf{M}^s_{ii}\boldsymbol{\phi}_{i,\xi}, \quad \xi = 1, 2, ..., N^s_i. \tag{5}$$

N^s_i is the number of interior DOFs for a sth substructure. N^s_m from Equation (4) denotes the number of selected dominant modes following the frequency cut-off method. This number should be smaller than the initial interior DOFs ($N^s_m < N^s_i$). The FINMs $\mathbf{\Phi}^s_{im}$ are derived from generalized eigenvalue analysis to satisfy the mass orthogonality, as follows:

$$[\mathbf{\Phi}^s_{im}]^T\mathbf{M}^s_{ii}\mathbf{\Phi}^s_{im} = \mathbf{I}_{mm}. \tag{6}$$

To obtain the static constraint modes for boundaries, a unit displacement is applied to the interface DOFs. In addition, an inertia force $\mathbf{f}^s_i$ is ignored for a static analysis.

$$\begin{bmatrix} \mathbf{K}^s_{ii} & \mathbf{K}^s_{ib} \\ \mathbf{K}^s_{bb} & \mathbf{K}^s_{bi} \end{bmatrix} \begin{bmatrix} \mathbf{\Psi}^s_{ii} \\ \mathbf{I}^s_{bb} \end{bmatrix} = \begin{bmatrix} \mathbf{0} \\ \mathbf{f}^s_b \end{bmatrix}, \tag{7}$$

The SCM is obtained by solving the upper part of Equation (7),

$$\mathbf{\Psi}^s_{ib} = -{\mathbf{K}^s_{ii}}^{-1}\mathbf{K}^s_{ib}. \tag{8}$$

The size of SCMs for sth substructure is N^s_b, which is equal to the number of initial physical interfaces. The boundary DOFs and compatibility are fully retained by static condensation to achieve direct synthesis.

According to the above procedures, the final CB transformation for a sth substructure is expressed as

$$\mathbf{T}^s = \begin{bmatrix} \mathbf{\Phi}^s_{im} & \mathbf{\Psi}^s_{ib} \\ \mathbf{0}_{bm} & \mathbf{I}_{bb} \end{bmatrix}. \tag{9}$$

The CB-reduced mass and stiffness matrices of a sth substructure are derived by applying transformations Equation (9) to the system matrices, such that

$$\begin{aligned} \bar{\mathbf{M}}^s &= [\mathbf{T}^s]^T \mathbf{M}^s \mathbf{T}^s = \begin{bmatrix} \mathbf{I}_{mm} & \bar{\mathbf{M}}^s_{mb} \\ \bar{\mathbf{M}}^s_{bm} & \check{\mathbf{M}}^s_{bb} \end{bmatrix}, \\ \bar{\mathbf{K}}^s &= [\mathbf{T}^s]^T \mathbf{K}^s \mathbf{T}^s = \begin{bmatrix} \mathbf{\Lambda}^s_{mm} & \mathbf{0}_{mb} \\ \mathbf{0}_{bm} & \check{\mathbf{K}}^s_{bb} \end{bmatrix}. \end{aligned} \tag{10}$$

The bar $(\bar{\cdot})$ and check $(\check{\cdot})$ notations indicate the matrices transformed into the reduced coordinate and the generalized coordinate, respectively. The total size of sth reduced subsystem is $N^s = N^s_i + N^s_b$.

The boundary DOFs retain continuity of each subsystem without reduction. According to the interface displacement compatibility, the reduced substructural system matrices are directly synthesized as follows:

$$\tilde{\mathbf{M}}_{bb} = \sum_{i=1}^{N_d} \check{\mathbf{M}}^i_{bb}, \quad \tilde{\mathbf{K}}_{bb} = \sum_{i=1}^{N_d} \check{\mathbf{K}}^i_{bb}. \tag{11}$$

The tilde $(\tilde{\cdot})$ notation denotes the synthesized system, and N_d is the number of substructures. Consequently, the final displacement and transformation relationship of coupled CB system matrices is

$$\begin{bmatrix} \mathbf{u}^1_m \\ \mathbf{u}^2_m \\ \vdots \\ \mathbf{u}^s_m \\ \mathbf{u}_b \end{bmatrix} = \mathbf{P} \begin{bmatrix} \bar{\mathbf{u}}^1_i \\ \bar{\mathbf{u}}^2_i \\ \vdots \\ \bar{\mathbf{u}}^s_i \\ \mathbf{u}_b \end{bmatrix}, \tag{12}$$

where

$$\mathbf{P} = \begin{bmatrix} \mathbf{\Phi}^1_{im} & 0 & 0 & 0 & 0 \\ & \mathbf{\Phi}^2_{im} & 0 & 0 & 0 \\ & & \ddots & 0 & \vdots \\ & & & \mathbf{\Phi}^s_{im} & 0 \\ \boldsymbol{symm} & & & & \mathbf{I} \end{bmatrix}. \tag{13}$$

The transformation $\mathbf{P}$ is used for system recovery to approximate the full system. The subscript im indicates the reduced interior subspace of the original CB method. More details and the overview of the original CB method are presented in Ref. [13].

3. Localized Interface Reduction

This section introduces the newly proposed interface-reduction method. The presented hybrid-level interface reduction can address the issues in terms of both accuracy and efficiency. In other words, the system-level interface reduction that CC modes are computed from the fully synthesized system may be inefficient sometimes, particularly when the system needs various design modifications. On the other hand, the local-level interface reduction disregarding system connectivity compromises accuracy. Moreover, enforcing interface compatibility, which is an initial consideration for synthesis after computing CC modes at the substructural level, is a challenging task. To address these issues, this localized interface method is developed based on the key idea of the hybrid-level interface reduction initially proposed by Krattiger et al. [38].

3.1. Interface Discrimination Algorithm for Independent Interface

According to the hybrid-level interface reduction, a single interface is constructed by coupling adjacent substructures. Nevertheless, this previous method is restricted to certain modelings where each interface is clearly segregated. However, as we usually adopt a graphic partitioning algorithm for an automatic division of the whole FE model, interfaces and their reduction cannot be handled considering design parameters. This issue becomes more critical for real applications with large numbers of DOFs. To overcome this limitation, the interface discrimination algorithm is proposed by assigning a unique number based on Boolean operations. Figure 1 illustrates differences in building interface sets depending on interface reduction techniques. In addition, the process for localizing interfaces using unique numbering is described in Table 1.

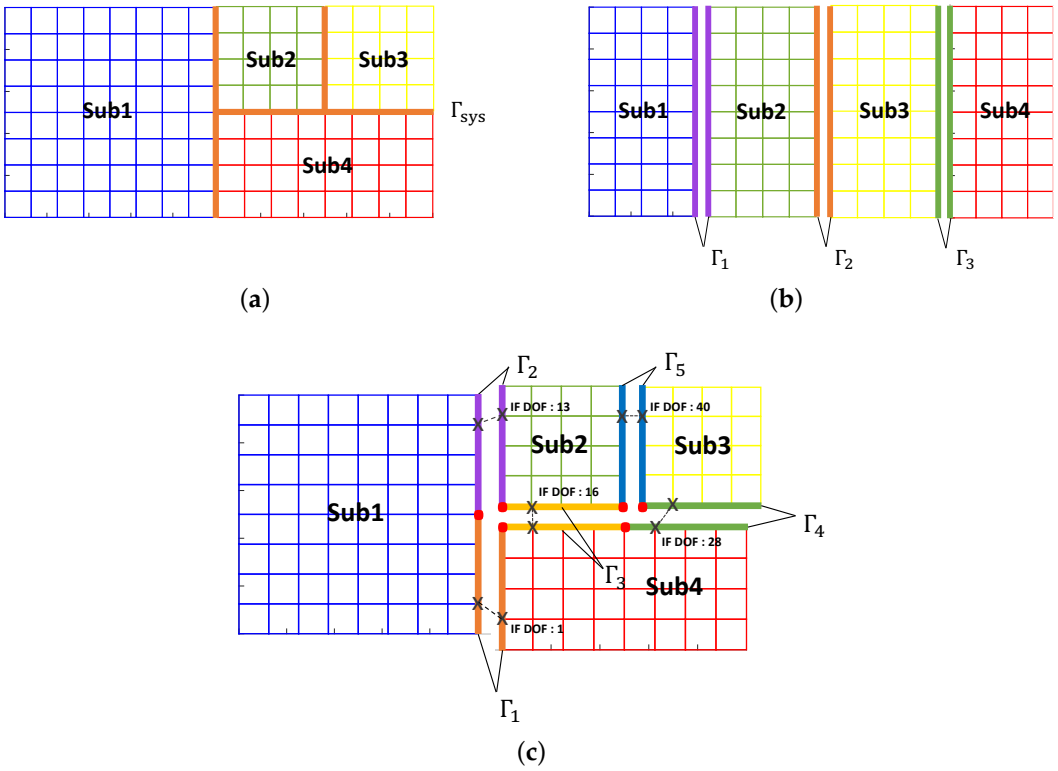

Figure 1. The comparison of interface reduction techniques between previous methods and proposed method. (**a**) System-level interface; (**b**) hybrid-level interface; (**c**) proposed semi-localized interface.

In Figure 1c, the red points are the one that contains three domains. To minimize accuracy loss, the red points sharing particularly many substructures are regarded as reduced interiors to retain without transformation. Therefore, they are excluded when we reduce the interface DOFs. Details of the algorithm for the interface discrimination are given in Algorithm 1. The example of converting binary to decimal numbers is presented in Table 1.

Table 1. Characteristic numbering for semi-localized interface reduction.

Interface DOF	Sub 1	Sub 2	Sub 3	Sub 4	Binary	Decimal	Interface Number
1	1	1	0	0	1100	12	Γ_1
13	0	1	0	1	0101	14	Γ_2
16	1	0	1	0	1010	10	Γ_3
28	0	1	1	0	0110	6	Γ_4
40	0	0	1	1	0011	3	Γ_5

Algorithm 1 Discrimination algorithm for interface localizing

1: **for** $s = 1, 2, ..., N_b$, **do**
2: Describe Boolean operations between interfaces and substructures.
3: Convert Boolean operations to a binary number.
4: Assign a unique number by converting a binary number to a decimal number.
5: **end for**
6: Discard untransformed points as numbering.
7: Rearrange interface numbering from 1 to j.

3.2. Interface Reduction Formulations

The interface is individually defined as a single set by the interface discrimination algorithm introduced in the above subsection. This implies that the proposed method conducts the secondary eigenvalue analysis to a partially synthesized system. In this section, the interface reduction process is described, and the jth localized interface Γ_j is presented in Figure 2 for comprehensive understanding.

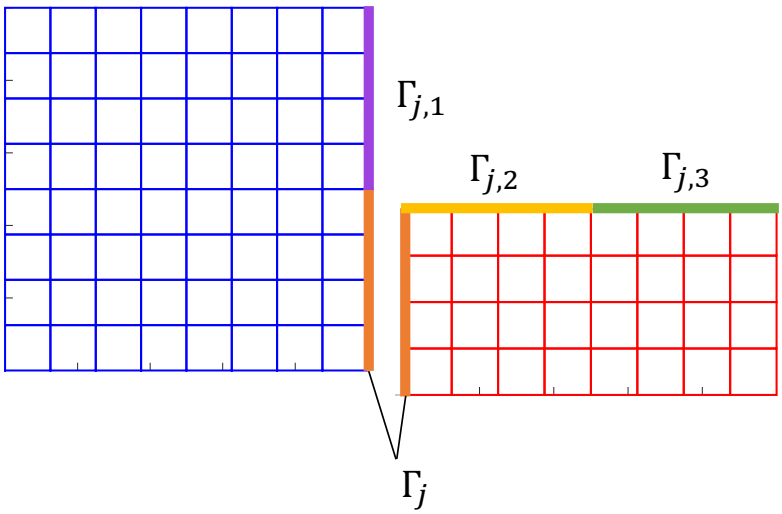

Figure 2. The jth localized interface Γ_j.

The system matrices of a jth interface are constructed by coupling relative substructures are

$$\tilde{\mathbf{M}}_{bb}^{\Gamma_j} = \sum_{i=1}^{N_k} \check{\mathbf{M}}_{bb}^{i}, \quad \tilde{\mathbf{K}}_{bb}^{\Gamma_j} = \sum_{i=1}^{N_k} \check{\mathbf{K}}_{bb}^{i}. \tag{14}$$

The N_k is the number of partially synthesized substructures to construct jth localized interface Γ_j. To obtain characteristic constraint modes, the secondary eigenvalue analysis is performed as

$$\mathbf{\Phi}_{bn}^{\Gamma_j} = [\boldsymbol{\phi}_{b,1}^{\Gamma_j}, \boldsymbol{\phi}_{b,2}^{\Gamma_j}, ..., \boldsymbol{\phi}_{b,N_n}^{\Gamma_j}], \tag{15}$$

where

$$\tilde{\mathbf{K}}_{bb}^{\Gamma_j} \boldsymbol{\phi}_{b,\xi} = \lambda_{b,\xi} \tilde{\mathbf{M}}_{bb}^{\Gamma_j} \boldsymbol{\phi}_{b,\xi}, \quad \xi = 1, 2, ..., N_b^{\Gamma_j}. \tag{16}$$

$N_b^{\Gamma_j}$ is the total number of boundary DOFs for a jth interface. The N_n is the number of selected CC modes to be used for interface reduction basis. According to modal reduction, the number of reduction basis should be $N_n < N_b^{\Gamma_j}$.

The range of CC modes computation is an important factor in obtaining guaranteed accuracy. The reduction basis for a jth interface (15) contains other interface sets dependent

on synthesized substructures. In Figure 2, for example, $\mathbf{\Gamma}_{j,1}, \mathbf{\Gamma}_{j,2}, \mathbf{\Gamma}_{j,3}, \mathbf{\Gamma}_{j,4}$ are uncompleted interface sets, and connected to substructures consist of $\mathbf{\Gamma}_j$:

$$\mathbf{\Phi}_{bn}^{\mathbf{\Gamma}_j} = \begin{bmatrix} \mathbf{\Phi}_{bj,n}^{\mathbf{\Gamma}_j} \\ \mathbf{\Phi}_{b1,n}^{\mathbf{\Gamma}_{j,1}} \\ \mathbf{\Phi}_{b2,n}^{\mathbf{\Gamma}_{j,2}} \\ \mathbf{\Phi}_{b3,n}^{\mathbf{\Gamma}_{j,3}} \end{bmatrix}. \tag{17}$$

Therefore, the proportion of interface set $\mathbf{\Phi}_{bj,n}^{\mathbf{\Gamma}_j}$ is only selected as an $\mathbf{\Gamma}_j$ reduction basis. The final interface reduction basis for a jth interface is expressed as

$$\mathbf{\Phi}_{kn}^{\mathbf{\Gamma}_j} = \left[\mathbf{\Phi}_{bj,n}^{\mathbf{\Gamma}_j} \right]. \tag{18}$$

Note that the additional sets are straightforwardly removed from Equation (17). However, it is crucial to consider these eliminated additional sets to account for the free-interface and rigid-body modes of partially synthesized systems.

In addition, the primary distinction between the previous hybrid level and this newly proposed localized interface reduction is that the points interconnected by multiple interfaces and substructures are discriminated, as presented in Figure 1a. Applying transformation to these red points may result in a significant loss of accuracy since the connection between interfaces and substructures are ignored. Thus, presented red points should be treated as CB-reduced interior DOFs and retained. Consequently, the relationship between interface-reduced CB systems is expressed as follows:

$$\begin{bmatrix} \mathbf{U}_m \\ \mathbf{U}_{ib} \\ \mathbf{U}_n^{\mathbf{\Gamma}} \end{bmatrix} = \begin{bmatrix} \mathbf{Q}_{im} & 0 & 0 \\ & \mathbf{I} & 0 \\ \boldsymbol{symm} & & \mathbf{Q}_{kn} \end{bmatrix} \begin{bmatrix} \bar{\mathbf{U}}_i \\ \mathbf{U}_{ib} \\ \bar{\mathbf{U}}_k^{\mathbf{\Gamma}} \end{bmatrix}, \tag{19}$$

where

$$\bar{\mathbf{U}}_i = \begin{bmatrix} \bar{\mathbf{u}}_i^1 \\ \bar{\mathbf{u}}_i^2 \\ \vdots \\ \bar{\mathbf{u}}_i^s \end{bmatrix}, \quad \mathbf{U}_{ib} = \begin{bmatrix} \mathbf{u}_i^1 \\ \mathbf{u}_i^2 \\ \vdots \\ \mathbf{u}_i^p \end{bmatrix}, \quad \bar{\mathbf{U}}_k^{\mathbf{\Gamma}} = \begin{bmatrix} \bar{\mathbf{u}}_k^{\mathbf{\Gamma}_1} \\ \bar{\mathbf{u}}_k^{\mathbf{\Gamma}_2} \\ \vdots \\ \bar{\mathbf{u}}_k^{\mathbf{\Gamma}_j} \end{bmatrix}. \tag{20}$$

Following to previous procedures, interface transformation bases, $\mathbf{Q}_{im}$ and $\mathbf{Q}_{kn}$, for a final interface localized system could be written as

$$\mathbf{Q}_{im} = \begin{bmatrix} \mathbf{\Phi}_{im}^1 & 0 & 0 & 0 \\ & \mathbf{\Phi}_{im}^2 & 0 & 0 \\ & & \ddots & 0 \\ & & & \mathbf{\Phi}_{im}^s \end{bmatrix}, \quad \mathbf{Q}_{kn} = \begin{bmatrix} \mathbf{\Phi}_{kn}^{\mathbf{\Gamma}_1} & 0 & 0 & 0 \\ & \mathbf{\Phi}_{kn}^{\mathbf{\Gamma}_2} & 0 & 0 \\ & & \ddots & 0 \\ & & & \mathbf{\Phi}_{kn}^{\mathbf{\Gamma}_j} \end{bmatrix}. \tag{21}$$

The $\mathbf{\Phi}_{im}^s$ is FINMs for interior reduction. p denotes numbering for retained points without transformation. $\mathbf{\Phi}_{kn}^{\mathbf{\Gamma}_j}$ indicates the localized CC modes for a jth interface.

This proposed localized interface-reduction method minimizes the trade-off between accuracy and efficiency in comparison to other techniques. Design modification respecting parameter changes is more effective than system-level interface reduction, which requires assembling all substructures for CC modes computation. As a result, interface parallel computation is also possible. Regarding accuracy, the connectivity of substructures can be

considered besides the local-level interface reduction, and enforcing compatibility is no longer required since straightforward synthesis can be allowed.

4. Numerical Examples

In this section, numerical examples are presented to evaluate the performance of the proposed interface-reduction method. One of the significant benefits of the proposed approach is that there is no modeling limitation to apply. To demonstrate the multiplicity of applicable models, the graphic partitioning algorithm METIS [39] is adopted for substructuring to design subdomains.

For performance verification, the original CB method [13] and the system-level interface reduced CB method with same proportion CC modes [24] are adopted as reference values. However, the previous hybrid-level interface reduction [38] cannot be applied to the systems substructured by METIS algorithm since this substructuring method provides complicated interface design, and users are not allowed to intervene for design modification. For fair comparison with the previous interface-reduction method, designed substructuring models are additionally presented with METIS substructuring. The relative error is written as

$$error_i = \frac{|\lambda_{FOM,i} - \lambda_{ROM,i}|}{\lambda_{FOM,i}}. \tag{22}$$

The subscript i denotes the ith eigenvalue of systems. Therefore, $\lambda_{FOM,i}$ indicates the ith modes of full-system, while $\lambda_{ROM,i}$ is the ith mode of the ROM . Note that the ROM could be the reference values and the proposed method. The performance evaluation of the presented systems is conducted by MATLAB R2022 in-house code under an 8-core Intel CPU running at 4.80 GHz. The finite element modeling information is summarized in Table 2. The materials for the presented structures are aluminum with the following properties: Young's modulus E = 72×10^9 Pa, Poisson ratio v = 0.33, and density $\rho = 27 \times 10^3$ kg/cm^3.

Table 2. DOF information of numerical examples.

	Elem.	Node	DOFs	FINMs	CC Modes	Designed ROM	METIS ROM
Plate	128	153	459	10%	30%	13.73%	14.16%
Box–beam	360	383	2298	5%	30%	8.40%	8.77%
Wing–box	12560	12073	72438	1%	10%	-	1.75%

4.1. Cantilever Plate

The cantilever plates divided into four substructures are presented. The four-node plate element is adopted for finite element modeling, and the total number of elements and DOFs are 128 and 459, respectively. In this plate example, designed substructuring is also presented and compared with METIS substructuring. Therefore, the number of interior and interface DOFs are slightly different, while the ratios of reduced systems are similar. The details of DOF information are also presented in Table 2. The domain decomposition information and localized interfaces are described in Figures 3 and 4 for the substructuring methods. Each substructure is dependent on certain design variables, such as the thickness of a plate. The thickness is 12 mm for all substructures for both structural models.

Figure 5 shows the error verification of the proportion of CC modes. To assess the accuracy of the proposed CC modes approaches, the number of CC modes is gradually reduced from 50% to 30%. Figure 5a represents the CC modes comparison for the system performed substructuring by designers. The entire system consists of four substructures, five localized interfaces, and two untransformed points, as presented in Figure 3. For the system reduction, 38 FINMs are used for interior reduction, which is about 10% of the entire interior DOFs. In addition, 29, 24, and 19 CC modes are employed for the interface reduction, which are 50%, 40%, and 30%, proportional to the entire interfaces, respectively. In general, noticeable error gaps are observed regarding the percentage of CC modes compared to the

original CMS. Nevertheless, the overall predictions are acceptable, with average relative errors of 0.3%, 1.9%, and 5.0% to the proportion of CC modes.

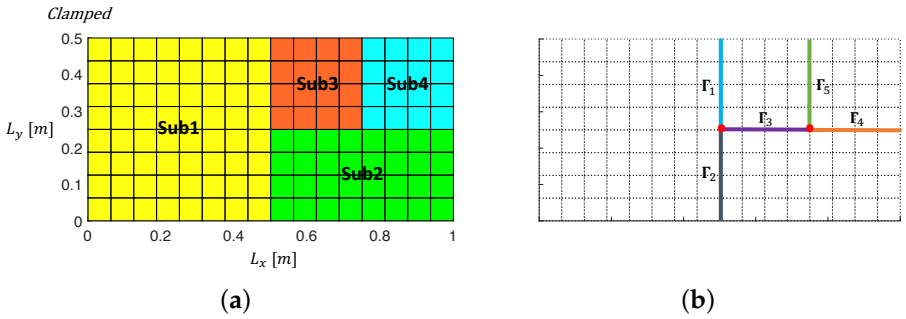

(**a**) (**b**)

Figure 3. Plate substructured by designation. (**a**) Plate with 4 design variables; (**b**) localized interfaces.

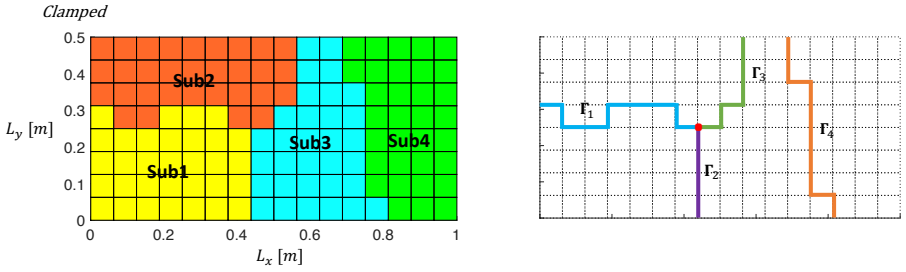

(**a**) (**b**)

Figure 4. Plate substructured by METIS. (**a**) Plate with 4 design variables; (**b**) localized interfaces.

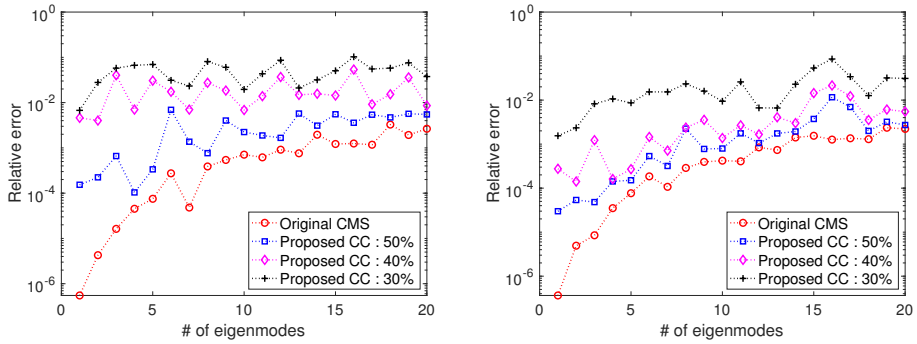

(**a**) (**b**)

Figure 5. Error verification with respect to the proportion of CC modes. (**a**) Designated substructuring plate; (**b**) METIS substructuring plate.

Regarding a plate structure performed substructuring by METIS in Figure 4, the entire system is composed of four substructures and four localized interfaces. There is an untransformed point, which is a connection of interface sets $\mathbf{\Gamma}_1$, $\mathbf{\Gamma}_2$, $\mathbf{\Gamma}_3$. The same percentage of modes are adopted for the reduction in both interiors and interfaces. The interior DOFs are reduced by 35 FINMs, and 46, 36, and 27 CC modes are, respectively, used to the presented proportion of CC modes. The average errors for 50%, 40%, and 30% CC modes are 0.2%, 0.4%, and 2.1%, respectively. A higher accuracy is noticed in METIS substructuring than in the designed substructures. However, those results could not guarantee that the METIS substructuring approach performs better than the designed system. This is due to the differences in the original number of interior and interface DOFs between the two modeling, as presented in Table 3. In this presented case, a larger number of CC modes are used than designed substructuring approaches. According to the characteristic of modal

system reduction, overall errors gradually increase as the number of CC modes increases, as expected, for both modeling cases.

Figure 6 compares the proposed methods and the system-level interface reduction. For a fair comparison, the total number of untransformed interface DOFs and the number of CC modes for each interface is equal to the applied number of system-level CC modes. The proposed methods show compromise in accuracy regardless of substructuring methods, while the system-level interface-reduction method presents great agreement with the original CB method. These accuracy losses are believed to be caused by system connectivity, partially considered, not a fully coupled system. Further investigation of accuracy will be presented by comparing with the previous hybrid-level interface-reduction methods in the following examples. Although the error gap is noticed, the proposed method demonstrates acceptable reliability, with presented relative errors at nearly 10^{-2}.

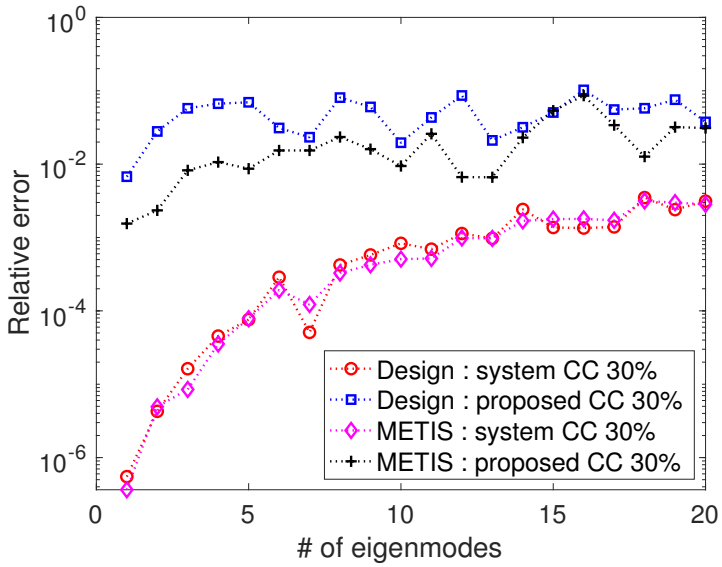

Figure 6. Error verification with respect to substructuring methods.

Table 3. The information of localized interfaces for plate.

	Interface DOFs	# of Interface Sets	Untransformed DOFs	# of CC Modes
Design domain	63	5	6	19
METIS: 4 subs	93	4	3	27

4.2. Shell Box–Beam

This section compares the performance of the proposed method with previous hybrid-level interface reduction techniques. To present the performance of the previous hybrid-level interface method, the box–beam structures are decomposed into the same number of subdomains with METIS substructuring, as illustrated in Figures 7 and 8. The system is designed to realize clearly isolated interface sets with multiple substructures, while the system designed by METIS substructuring has interconnected localized interface sets and substructures, as shown in Figure 8.

Furthermore, the applicable modeling range is also investigated with diverse box–beam substructuring designs. For FE modeling, 360 4-node flat shell elements (MITC4) [41] and 383 nodes are employed. The initial thickness is 25 mm for all presented beam models and substructures. The FE modeling details are presented by comparison of FOM and ROM in Table 2.

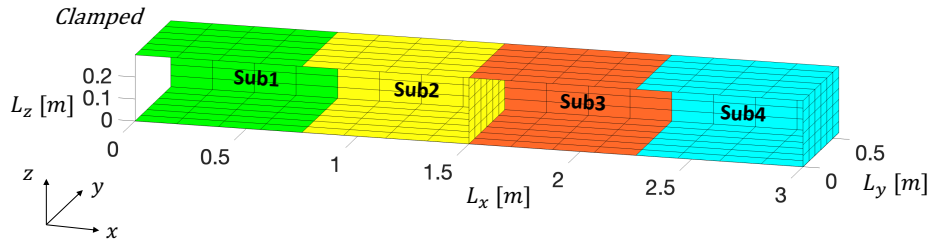

(**a**)

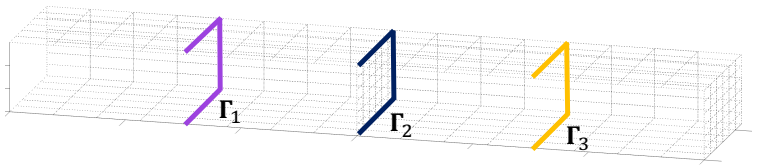

(**b**)

Figure 7. Box–beam substructured by designation. (**a**) Box–beam with 4 design variables; (**b**) localized interfaces.

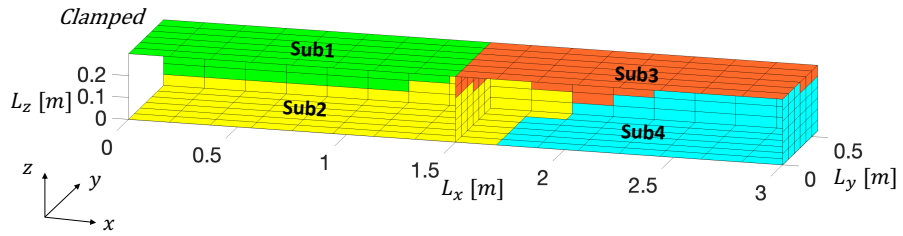

(**a**)

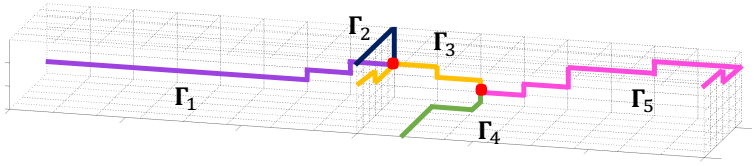

(**b**)

Figure 8. Box–beam substructured by METIS. (**a**) Box–beam with 4 design variables; (**b**) localized interfaces.

Figure 9 presents the error verification with respect to the proportion of CC modes for the box–beam structure. According to Figure 7, four substructures construct three independent interface sets without untransformed points to represent a modeling case applicable to the previous hybrid-level evaluation. The relative errors of the structure, which is distinctly sectioned, are presented in Figure 9a. Despite of error discrepancy in lower modes, the overall error level is comparable with the original CB method. Additionally, relative errors within 20 modes are below 10^{-3} for all presented numbers of CC modes.

In addition, Figure 9b shows the relative errors for the system performed substructuring by METIS. Compared to the original CB method, the relative errors steadily increase by considering the number of CC modes. This is a reasonable trend of modal reduction. When 30% of CC modes are used for reduction, the average relative error is 0.17%, while for 50% and 40% of CC modes, the relative errors are all below 10^{-3}.

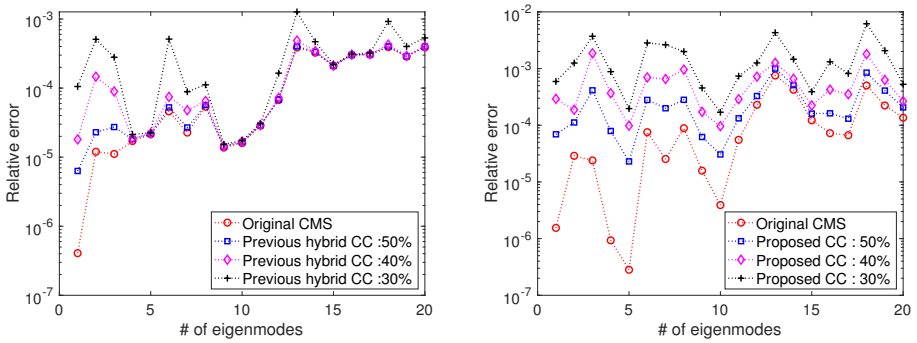

Figure 9. Error verification with respect to the proportion of CC mods for box–beam. (**a**) Previous hybrid interface reduction; (**b**) proposed localized interface reduction.

Corresponding to the previous investigation determining an appropriate number of CC modes for the box beam, it turned out that employing 30% of CC modes can achieve the desired error level, which is below 10^{-2} for the presented box model. Accordingly, the previous and proposed hybrid-level CC modes are compared using 30% CC modes in Figure 10. Furthermore, the system-level interface reduced system is also presented for more comprehensive evaluation. The proposed method shows a higher error level than the previous hybrid-level interface reduction. However, this discrepancy could not be evidence to conclude that the proposed method causes a larger compromise in accuracy than the previous method. This is because the modeling condition, such as the numbers of interior and interface DOFs, differs even when the same proportion of CC modes are employed. For instance, 102 and 95 CC modes are, respectively, selected as the 30% CC modes for both designed and METIS substructuring models. The information on localized interfaces for the beam is summarized in Table 4. According to this comparison, it can be inferred that larger accuracy losses compared to the identical number of system-level CC modes are influenced by the partial system coupling, even though a perfectly fair comparison between the proposed and previous hybrid-level is not possible.

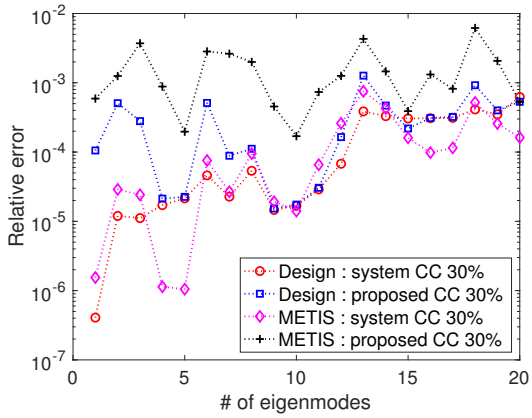

Figure 10. Error verification with respect to substructuring methods.

In Figure 11, additional beam models that have different numbers of substructures are presented for further investigation of applicable modeling ranges with METIS substructuring. In each case, a consistent 30% proportion of CC modes is employed for each localized interface set. The system defined by 6 substructures and 10 interfaces selects 144 CC modes, while the total interface DOFs are 480, in Figure 11a. Regarding the system with 8 substructures in Figure 11b, substructures build 11 localized interfaces, and 170 CC

modes are selected from 594 original interface DOFs. More details of the localized interfaces and untransformed DOFs are presented in Table 4.

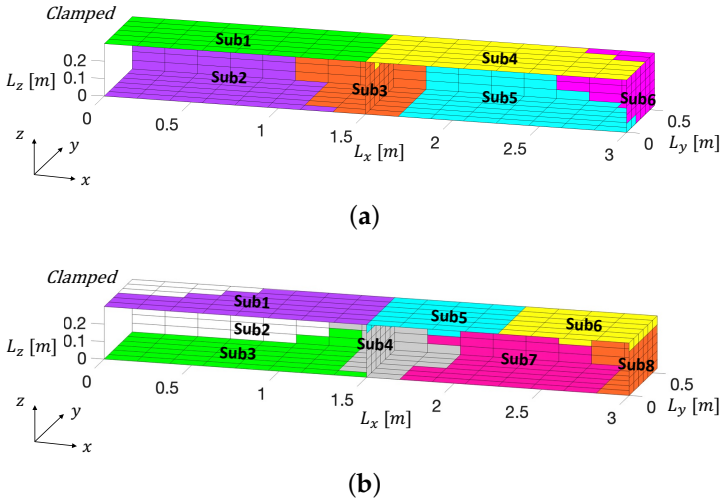

Figure 11. METIS design. (**a**) 6 substructuring; (**b**) 8 substructuring.

Table 4. The information of localized interfaces for box–beam.

	Interface DOFs	# of Interface Sets	Untransformed DOFs	# of CC Modes
Design domain	342	3	-	102
METIS: 4 subs	330	5	12	95
METIS: 6 subs	480	10	18	144
METIS: 8 subs	594	11	42	170

Figure 12 presents the relative error comparison with respect to the number of substructures. When the system has four substructures, relative error within 20 modes shows great prediction with figures below 10^{-3}. On the other hand, error levels with a larger number of substructures rise, even the average relative errors are still acceptable as 0.95% and 2.23% for six and eight substructures, respectively. It is important to note that the same percentage of CC modes is applied to each localized interface set for reduction. This implies that the influence of each interface on the entire system is overlooked in this investigation. Consequently, the sensitivity analysis of each interface set would be a possible option to improve the accuracy of the proposed method.

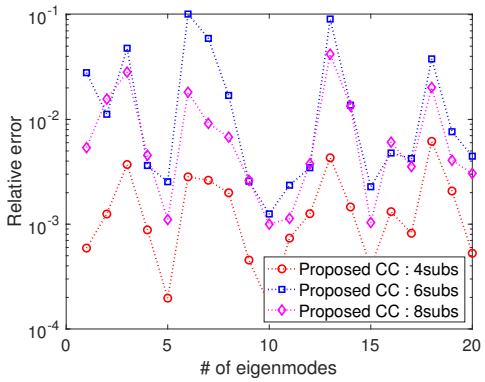

Figure 12. Error verification with respect to the number of substructures.

4.3. Wing Box

The systems presented above are unsuitable to properly demonstrate the efficiency of the proposed method due to their inherently low number of DOFs. Moreover, interface reduction is carried out under limited conditions, with over 30% of CC modes proportional to entire interface DOFs. This limitation arises from the need to include rigid body modes, aiming for higher system reduction than 30% CC modes cannot sufficiently contain rigid body modes.

Accordingly, a large-winged structure with numerous substructures and interfaces is presented as a final example in Figure 13. All substructures in this structure have the same thickness value of 8 mm. The structure consists of 12,560 shell elements and 12,073 nodes, with specific DOFs detailed in Table 2. The system is divided into 10 substructures and 28 localized interfaces by METIS substructuring, as indicated in Table 5. This section focuses on efficiency verification, not only accuracy. Therefore, parametric studies were also performed to evaluate the performance.

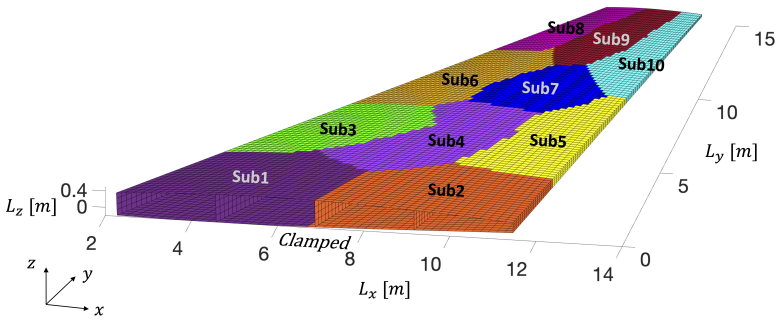

Figure 13. Wing–box modeling.

Table 5. The information of localized interfaces for wing.

	Interface DOFs	# of Interface Sets	Untransformed DOFs	# of CC Modes
Large wing	5184	28	24	578

Figure 14 presents a relative comparison with respect to the percentage of CC modes for wing structures. The relative errors consistently increase, similar to the previous investigations. When 1076 and 1586 CC modes are applied, which is proportional 20% or 30% to entire interface DOFs, reliable error levels are observed with the value of relative errors are approximately 10^{-3}. However, applying 10% CC modes compared to the entire interface DOFs shows 10^{-2} error level, while the system-level method shows great accuracy below 10^{-4}. Nonetheless, the average relative error remains below 1%, specifically at 0.92%.

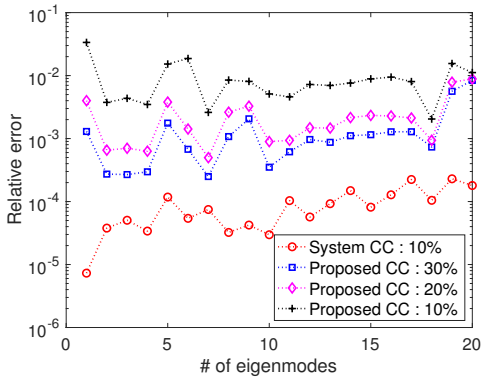

Figure 14. Error verification with respect to CC modes.

To assess the efficiency of the proposed method, the eigenvalue analysis is conducted by using *eigs* function [42] adopted in MATLAB due to significant computational resources. As shown in Figure 15, three values of computation time are presented: full-system, original CMS without interface reduction, and the system reduced using the proposed CC modes method. Despite a considerable interior reduction, there is no significant difference in system computation time between the full system and the original CMS system. On the other hand, the system that employed CC modes shows a great decrease in computation time to 0.12 s. Significant time saving can be achieved with this proposed method—approximately 5.19% of system solving time is taken compared to the original CMS.

For specific comparison in efficiency, the system matrices for CC modes comparison between the system-level and proposed method are presented in Figure 16. Interface region accounting for CC modes computation is marked with a yellow box on the sparsity matrix. Figure 16b–d show partially synthesized stiffness matrices to construct semi-localized interfaces which numbers 1, 2, and 3, and Figure 16a offers the stiffness matrix, which is fully synthesized all substructures. For the system-level interface reduction, the CC modes were computed by considering the system matrix, which has a 9,865,565 non-zero value. On the other hand, the proposed method handles 1,470,616, 1,961,465, and 3,645,419 non-zero matrices for CC modes computation, respectively.

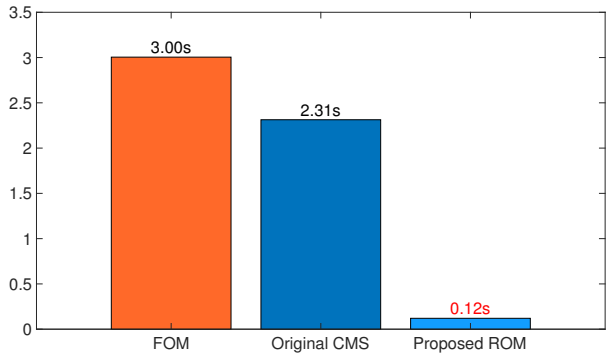

Figure 15. System solving time for wing.

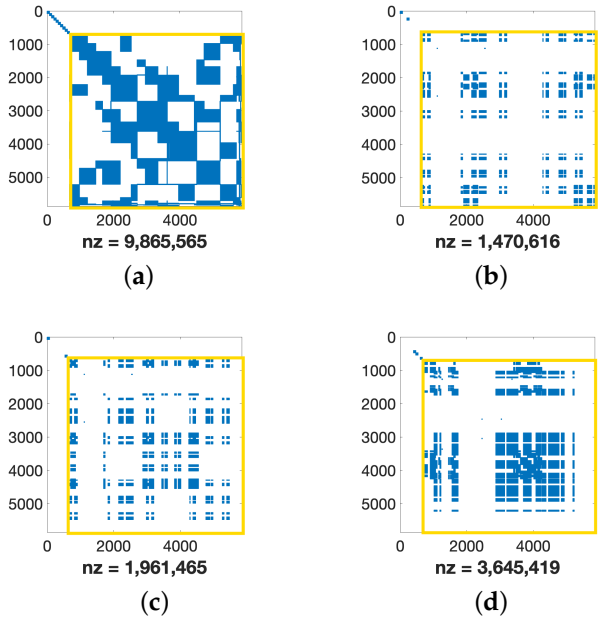

Figure 16. CC modes computation comparison. (**a**) System-level CC modes; (**b**) proposed cc modes—interface 1; (**c**) proposed CC modes: interface 2; (**d**) proposed CC modes: interface 3.

According to the interface matrices comparison presented in Figure 16, the CC modes computation time comparison is also provided in Figure 17. The orange bar represents the secondary eigenvalue analysis time for system-level CC modes computation, while the blue bars indicate individual localized interfaces determined by the proposed method. Most of the localized interfaces require less than 200 s for CC modes computation except for the 13th and 23rd interfaces, while the system-level takes 1066 s. Additionally, this figure also points out that this proposed method enables parallel computation for each interface set. Only several interfaces connected to substructures requiring design modification are considered for design changes, not the full size of the system interface.

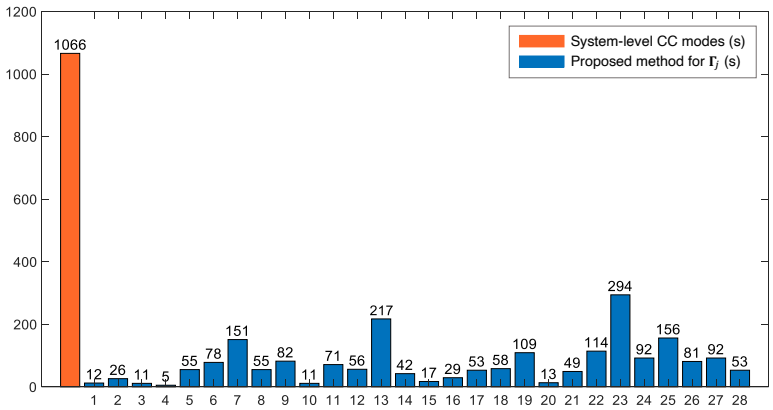

Figure 17. CC modes computation time with respect to each interface.

For further efficiency verification, simple parametric studies have been conducted in this section considering two case scenarios. The thickness of marked substructures varies as [8,10,12] mm, while the previous performance evaluations input consistent thickness for all substructures. The second and eighth substructures are considered for parametric variations following Figure 18a. For the system-level CC modes computation, $3 \times 3 = 9$ times secondary eigenvalue analysis is performed on a fully coupled system. On the contrary, eight semi-localized interface sets are associated with parameter-varied substructures. Therefore, $8 \times 3 = 24$ times CC modes are computed in partially assembled systems. For three substructures with parametric variations according to Figure 18b, the third substructure and five semi-localized interfaces are additionally accounted for CC modes computation; $3 \times 3 = 27$ times and $13 \times 3 = 39$ times secondary eigenvalue analysis are, respectively, performed for system-level and proposed interface-reduction method. The substructure information for constructing each semi-localized interface $\mathbf{\Gamma}_j$ is shown in Table 6.

Figure 19 shows the CC modes computation time comparison for each parametric case studies case. Case 1 represents parametric studies for two substructures shown in Figure 19a, and the system-level CC modes computation took 9592.62 s, including nine repeated computations. Meanwhile, the proposed CC modes computation takes 949.05 s, which is less than 10% compared to the system-level CC modes computation time. Furthermore, in parametric study case 2, the proposed method requires 1944.50 s, while the system-level case takes 28,777.87 s. This figure indicates that approximately 6% of computation time is consumed in comparison to the system-level computation. One of the most significant benefits of the proposed method is the availability of parallel computation. Therefore, only the most time-consuming interface associated with parametric variations is accounted for computation. As a result, it can be expected to achieve at least 61 times computational resource savings according to case 2, which has three parametric varied substructures, when more substructures are associated with parametric studies. The efficiency of CC modes computation with respect to presented parametric studies cases is organized in Tables 7 and 8.

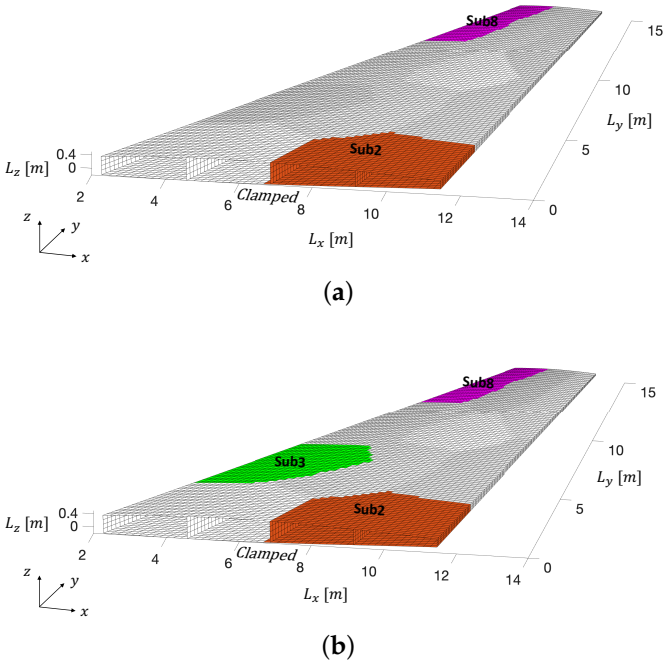

Figure 18. Parametric case studies. (**a**) Case 1: 2 substructure varied to parametric variations; (**b**) Case 2: 3 substructure varied to parametric variations.

Table 6. Adjacent substructures to construct interface Γ_j.

	Localized-Interface Number Γ_j												
	1	**2**	**3**	**4**	**6**	**10**	**17**	**18**	**20**	**25**	**26**	**27**	**28**
Subdomains connectivity	-	-	-	1, 2	1, 2, 4	2, 5	2, 4	-	-	-	-	2, 4, 5	-
	-	3, 6	1, 3	-	-	-	-	3, 4	-	3, 4, 6	1, 3, 4	-	-
	6, 8	-	-	-	-	-	-	-	8, 9	-	-	-	7, 8

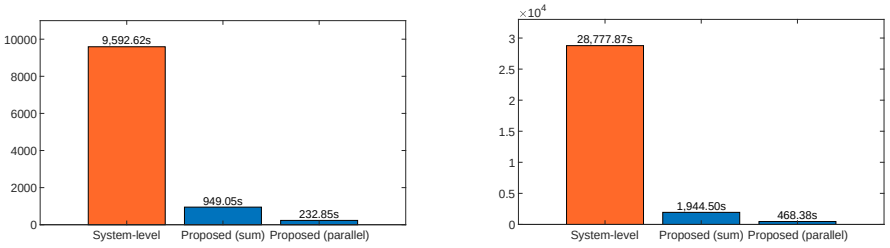

Figure 19. CC modes computation time comparison. (**a**) Computation time for case 1; (**b**) Computation time for case 2.

Table 7. CC modes computation time comparison: 2subs parametric variations.

	System-Level	**Proposed Method (Sum)**	**Proposed (Parallel)**
# of CC modes computation	9	24	3
CC modes computation time	9,592.62 s	949.05 s	232.85 s

Table 8. CC modes computation time comparison: 3subs parametric variations.

	System-Level	Proposed Method (Sum)	Proposed (Parallel)
# of CC modes computation	27	39	3
CC modes computation time	28,777.87 s	1,944.50 s	468.38 s

5. Conclusions

In this paper, an enhanced hybrid-level interface-reduction method was proposed by developing an interface localization algorithm. Although the previous CMS and its variants allow convenient parametric studies by decomposing the main structure into independent subsystems, the methods were limited in using ROM for parametric variations as they primarily focused on the interior reduction, and as a result, the final ROMs were not online-capable size. Since interface reduction is mandatory to be useful for efficient computation, various interface-reduction methods were continuously developed by incorporating secondary eigenvalue analysis. Among them, the methods adopting hybrid-level characteristic constraint (CC) modes verify the feasibility of considering design modifications at the substructural level without much accuracy loss. The proposed method overcomes the limitation of previous hybrid-level interface reduction. Specifically, the previous methods were only applicable to independently defined interfaces and subsystems. In the present work, the interface localization was realized by assigning unique numbers based on substructural-level Boolean operations. As a result, the substructuring and interface reduction became possible regardless of the number of interconnected interfaces and substructures. The performance of the proposed method was demonstrated for both accuracy and efficiency aspects. Compared with the methods at the system-level CC modes, the proposed one requires less than 10 times the CC mode computation time, resulting in a significant enhancement in the efficiency of the constructing ROM for the parametric studies of large dynamical systems.

As a future development, the proposed interface localization method will be applicable to the family of parametric CMS methods. The conventional parametric CMS derives ROMs and their solutions for parametric variations in the online stage by using precomputed offline samples with reduced subsystems. Therefore, the proposed interface localizing method is expected to discard the interface reduction process in the online stage, whereas the previous CMS performs the secondary eigenvalue analysis in the online stage. Additionally, this proposed method is expected to apply to the finite volume method (FVM) expending from the FEM analysis [42–45].

Author Contributions: S.C.: conceptualization, data curation, formal analysis, investigation, methodology, software, validation, visualization, writing—original draft preparation. J.L.: conceptualization, funding acquisition, investigation, methodology, resources, software, supervision, writing—review and editing. All authors have read and agreed to the published version of the manuscript.

Funding: This research was supported by the National Research Foundation of Korea, 2020 (NRF-2020R1C1C1011970), and by the National Research Foundation of Korea (NRF) grant funded by the Korean government (MSIT) (NRF-2018R1A5A7023490).

Data Availability Statement: Data available on request, subject to privacy or ethical considerations.

Conflicts of Interest: The authors declare no conflict of interest.

References

1. Amsallem, D.; Farhat, C. Interpolation method for adapting reduced-order models and application to aeroelasticity. *AIAA J.* **2008**, *46*, 1803–1813. [CrossRef]
2. Amsallem, D.; Farhat, C. An Online Method for Interpolating Linear Parametric Reduced-Order Models. *SIAM J. Sci. Comput.* **2011**, *33*, 2169–2198. [CrossRef]

3. Bui-Thanh, T.; Willcox, K.; Ghattas, O. Model Reduction for Large-Scale Systems with High-Dimensional Parametric Input Space. *SIAM J. Sci. Comput.* **2008**, *30*, 3270–3288. [CrossRef]
4. Negri, F.; Manzoni, A.; Amsallem, D. Efficient model reduction of parametrized systems by matrix discrete empirical interpolation. *J. Comput. Phys.* **2015**, *303*, 431–454. [CrossRef]
5. Lee, J.; Cho, M. An interpolation-based parametric reduced order model combined with component mode synthesis. *Comput. Methods Appl. Mech. Eng.* **2017**, *319*, 258–286. [CrossRef]
6. Lee, J. A parametric reduced-order model using substructural mode selections and interpolation. *Comput. Struct.* **2019**, *212*, 199–214. [CrossRef]
7. Lee, J. A dynamic substructuring-based parametric reduced-order model considering the interpolation of free-interface substructural modes. *J. Mech. Sci. Tech.* **2018**, *32*, 5831–5838. [CrossRef]
8. Zhou, Z.; Zhang, H.; Yang, X. H1-norm error analysis of a robust ADI method on graded mesh for three-dimensional subdiffusion problems. *Numer. Algo.* **2023**, 1–19. [CrossRef]
9. Zhang, H.; Liu, Y.; Yang, X. An efficient ADI difference scheme for the nonlocal evolution problem in three-dimensional space. *J. Appl. Math. Comput.* **2023**, *69*, 651–674. [CrossRef]
10. Tian, Q.; Yang, X.; Zhang, H.; Xu, D. An implicit robust numerical scheme with graded meshes for the modified Burgers model with nonlocal dynamic properties. *Comp. Appl. Math.* **2023**, *42*, 246. [CrossRef]
11. Wang, W.; Zhang, H.; Jiang, X.; Yang, X. A high-order and efficient numerical technique for the nonlocal neutron diffusion equation representing neutron transport in a nuclear reactor. *Ann. Nucl. Energy* **2024**, *195*, 110163. [CrossRef]
12. Hurty, W. Dynamic analysis of structures using substructure modes. *AIAA J.* **1965**, *3*, 678–685. [CrossRef]
13. Craig, R.R.; Bampton, M.C.C. Coupling of substructures for dynamic analyses. *AIAA J.* **1968**, *6*, 1313–1319. [CrossRef]
14. Bennighof, J.K.; Lehoucq, R.B. An automated multilevel substructuring method for eigenspace computation in linear elastodynamics. *SIAM J. Sci. Comput.* **2004**, *25*, 2084–2106. [CrossRef]
15. Kim, J.G.; Lee, P.S. An enhanced craig–bampton method. *Int. J. Numer. Methods Eng.* **2015**, *103*, 79–93. [CrossRef]
16. Craig, R.R.; Kurdila, A.J. *Fundamentals of Structural Dynamics*; John Wiley & Sons: Hoboken, NJ, USA, 2006.
17. Craig, R.R. Substructure Methods in Vibration. *J. Vib. Acoust.* **1995**, *117*, 207–213. [CrossRef]
18. de Klerk, D.; Rixen, D.J.; Voormeeren, S.N. General Framework for Dynamic Substructuring: History, Review and Classification of Techniques. *AIAA J.* **2008**, *46*, 1169–1181. [CrossRef]
19. Peskin, C.S. Numerical analysis of blood flow in the heart. *J. Comput. Phys.* **1977**, *25*, 220–252. [CrossRef]
20. Zhang, L.; Gerstenberger, A.; Wang, X.; Liu, W.K. Immersed finite element method. *Comput. Methods Appl. Mech. Eng.* **2004**, *193*, 2051–2067. [CrossRef]
21. Babuška, I.; Banerjee, U.; Kergrene, K. Strongly stable generalized finite element method: Application to interface problems. *Comput. Methods Appl. Mech. Eng.* **2017**, *327*, 58–92. [CrossRef]
22. Zhang, Q.; Babuška, I. A stable generalized finite element method (SGFEM) of degree two for interface problems. *Comput. Methods Appl. Mech. Eng.* **2020**, *363*, 112889. [CrossRef]
23. Craig , R.R., Jr.; Chang, C.J. *Substructure Coupling for Dynamic Analysis and Testing*; Technical Report; NASA: Washington, DC, USA, 1977.
24. Castanier, M.P.; Tan, Y.C.; Pierre, C. Characteristic constraint modes for component mode synthesis. *AIAA J.* **2001**, *39*, 1182–1187. [CrossRef]
25. Tran, D. Component mode synthesis methods using interface modes. Application to structures with cyclic symmetry. *Comput. Struct.* **2001**, *79*, 209–222. [CrossRef]
26. Tran, D.M. Component mode synthesis methods using partial interface modes: Application to tuned and mistuned structures with cyclic symmetry. *Comput. Struct.* **2009**, *87*, 1141–1153. [CrossRef]
27. Herrmann, J.; Maess, M.; Gaul, L. Substructuring including interface reduction for the efficient vibro-acoustic simulation of fluid-filled piping systems. *Mech. Syst. Signal Process.* **2010**, *24*, 153–163. [CrossRef]
28. Cammarata, A.; Sinatra, R.; Maddìo, P.D. Interface reduction in flexible multibody systems using the Floating Frame of Reference Formulation. *J. Sound Vib.* **2022**, *523*, 116720. [CrossRef]
29. Hughes, P.J.; Kuether, R.J. Nonlinear Interface Reduction for Time-Domain Analysis of Hurty/Craig Bampton Superelements with Frictional Contact. *J. Sound Vib.* **2021**, *507*, 116154. [CrossRef]
30. Monteil, M.; Besset, S.; Sinou, J.J. A double modal synthesis approach for brake squeal prediction. *Mech. Syst. Signal Process.* **2016**, *70–71*, 1073–1084; [CrossRef]
31. Lindberg, E.; Hörlin, N.E.; Göransson, P. Component mode synthesis using undeformed interface coupling modes to connect soft and stiff substructures. *Shock Vib.* **2013**, *20*, 157–170. [CrossRef]
32. Lee, S.; Mok, H.; Kim, C.W. On a component mode synthesis on multi-level and its application to dynamics analysis of vehicle system supported with spring-stiffness damper system. *J. Mech. Sci. Tech.* **2011**, *25*, 3115–3121. [CrossRef]
33. Hong, S.K.; Epureanu, B.I.; Castanier, M.P. Next-generation parametric reduced-order models. *Mech. Syst. Signal Process.* **2013**, *37*, 403–421. [CrossRef]
34. Kuether, R.J.; Allen, M.S.; Hollkamp, J.J. Modal Substructuring of Geometrically Nonlinear Finite Element Models with Interface Reduction. *AIAA J.* **2017**, *55*, 1695–1706. [CrossRef]

35. Holzwarth, P.; Eberhard, P. Interface Reduction for CMS Methods and Alternative Model Order Reduction. *IFAC-PapersOnLine* **2015**, *48*, 254–259. [CrossRef]
36. Wu, L.; Tiso, P.; Van Keulen, F. Interface reduction with multilevel Craig Bampton substructuring for component mode synthesis. *AIAA J.* **2018**, *56*, 2030–2044. [CrossRef]
37. Aoyama, Y.; Yagawa, G. Component mode synthesis for large-scale structural eigenanalysis. *Comput. Struct.* **2001**, *79*, 605–615. [CrossRef]
38. Krattiger, D.; Wu, L.; Zacharczuk, M.; Buck, M.; Kuether, R.J.; Allen, M.S.; Tiso, P.; Brake, M.R. Interface reduction for Hurty/Craig Bampton substructured models: Review and improvements. *Mech. Syst. Signal Process.* **2019**, *114*, 579–603. [CrossRef]
39. Karypis, G.; Kumar, V. *METIS: A Software Package for Partitioning Unstructured Graphs, Partitioning Meshes, and Computing Fill-Reducing Orderings of Sparse Matrices*; University of Minnesota: Minneapolis, MN, USA, 1997.
40. Bathe, K.J. *Finite Element Procedures*; Pearson Education: London, UK, 2006.
41. Dvorkin, E.N.; Bathe, K.J. A continuum mechanics based four-node shell element for general non-linear analysis. *Eng. Comput.* **1984**, *1*, 77–88; [CrossRef]
42. Radke, R.J. *A Matlab Implementation of the Implicitly Restarted Arnoldi Method for Solving Large-Scale Eigenvalue Problems*; Rice University: Houston, TX, USA, 1996.
43. Yang, X.; Zhang, H. The uniform l1 long-time behavior of time discretization for time-fractional partial differential equations with nonsmooth data. *Appl. Math. Lett.* **2022**, *124*, 107644. [CrossRef]
44. Yang, X.; Zhang, H.; Zhang, Q.; Yuan, G. Simple positivity-preserving nonlinear finite volume scheme for subdiffusion equations on general non-conforming distorted meshes. *Nonlinear Dyn.* **2022**, *108*, 3859–3886. [CrossRef]
45. Yang, X.; Zhang, H.; Zhang, Q.; Yuan, G.; Sheng, Z. The finite volume scheme preserving maximum principle for two-dimensional time-fractional Fokker–Planck equations on distorted meshes. *Appl. Math. Lett.* **2019**, *97*, 99–106. [CrossRef]

Disclaimer/Publisher's Note: The statements, opinions and data contained in all publications are solely those of the individual author(s) and contributor(s) and not of MDPI and/or the editor(s). MDPI and/or the editor(s) disclaim responsibility for any injury to people or property resulting from any ideas, methods, instructions or products referred to in the content.